8.11 VARIABILITY OF OCEAN SKIN TEMPERATURE FROM AIRBORNE INFRARED IMAGERY DURING CBLAST-LOW

Christopher J. Zappa*
Lamont-Doherty Earth Observatory, Columbia University, Palisades, NY

Andrew T. Jessup
Applied Physics Laboratory, University of Washington, Seattle, WA

1. INTRODUCTION

Airborne infrared (IR) remote sensing techniques have been shown to quickly characterize the spatial and temporal scales of ocean skin temperature as well as a wide variety of processes that are important to the variability of air-sea fluxes of heat, mass, and momentum. Results from Tropical Ocean-Global Atmosphere, Coupled Ocean-Atmosphere Response Experiment (TOGA-COARE) have demonstrated the importance of skin temperature in air-sea interaction. Accurate knowledge of the skin temperature has been shown to be critical to estimating surface fluxes [*Fairall et al.*, 1996] and as a result its spatial variability influences the small-scale distribution of those fluxes [*Hagan et al.*, 1997; *Walsh et al.*, 1998]. The focus of our observations is the spatial variability of the ocean surface skin temperature under low wind conditions.

Results reported by [*Hagan et al.*, 1997] were derived from airborne measurements made with a narrow field-of-view (FOV) infrared (IR) radiometer. The high-noise limitation of radiometry from aircraft requires significant spatial averaging to reduce the noise. [*Hagan et al.*, 1997]They reported an effective spatial resolution of 100 m with a resulting temperature resolution of 0.1°C. For wind speeds less than 4 m s^{-1}, they found diurnal warming of the skin layer that preceded subsequent increases in subsurface temperature. Horizontal gradients of 1°C in 10 km were observed under conditions of low wind and high solar insolation. Cool patches due to rainfall resulted in gradients of similar magnitude. They also reported evidence of cloud "imprints," whereby shadowing by the clouds produce corresponding regions of cooler skin temperature. They suggested that "SST maxima on scales of 10-15 km enhance the transfer of moisture in the boundary layer by natural convection." [*Walsh et al.*, 1998] reported on similar measurements made from a different aircraft along with measurements of mean square wave slope. They observed horizontal variability in skin temperature on 5-km scales that was anticorrelated with mean square slope. The patterns propagated with a speed and direction that was similar to internal gravity waves detected by moorings. They suggested that coupling between the internal waves and the dirurnal surface layer might be responsible for their observations.

An early demonstration of the potential of IR imagery of the ocean surface from aircraft was reported by [*McAlister and McLeish*, 1965]. They performed some of the first measurements of the horizontal structure of ocean skin temperature using an IR scanner and recorded signatures of apparent fronts, large-scale ocean eddies, free-convective patterns, wind streaks, and whitecapping. However, there were no upper ocean measurements to corroborate the processes that occurred. [*Peltzer et al.*, 1987] used an airborne IR imaging system for the detection of ship wakes during the day, when the diurnal thermocline was well established. The thermal wake signatures recorded by the imaging system depict the contrast between the cool center of the ship wake produced by the upwelling of the underlying water and a warmer undisturbed surface layer. Smaller-scale process studies of ocean skin temperature have demonstrated the effect of deep-water breaking waves [*Jessup et al.*, 1997a], free-convective patchiness [*Zappa et al.*, 1998], microscale wave breaking [*Jessup et al.*, 1997b], and deep-water swell [*Jessup and Hesany*, 1996] on the ocean skin layer, which is often cooler than the underlying water [*Katsaros*, 1980b]. These measurements using IR imagery

* *Corresponding author address*: Christopher J. Zappa, Lamont-Doherty Earth Observatory, Columbia University, 61 Route 9W, Palisades, NY 10964; email: zappa@ldeo.columbia.edu

highlight a portion of the variety of processes that affect the ocean skin temperature.

Here, we report on the spatial variability of ocean surface temperature using airborne infrared measurements during the field campaign of the Coupled Boundary Layers, Air-Sea Transfer in Low Winds (CBLAST-Low) Experiments in 2002 and 2003. The extensive spatial coverage and fine spatial and temperature resolution of our systems allows us to examine spatial scales in skin temperature from processes that span the atmospheric boundary layer of *O*(1km) down to wave-related processes *O*(1m). We produced thermal maps of the study site using time series of ocean skin temperature and compared these with the fine-scale structures observed within the IR imagery to investigate a variety of processes with varying scales in the coastal zone. We combine the airborne IR data with upper ocean measurements to relate horizontal variability in surface skin temperature to sub-surface phenomena.

2. CBLAST-LOW EXPERIMENTS

Measurements of ocean skin temperature variability were made during the main field campaigns of the CBLAST-Low (Coupled Boundary Layers, Air-Sea Transfer in Low Winds) experiment in August/September 2002 and July/August 2003 off the south coast of Martha's Vineyard. Central to the CBLAST-LOW site were the offshore tower [*Edson et al.*, 2004] and horizontal ocean buoy array [*Farrar et al.*, 2004]. We flew a state-of-the-art, high spatial resolution, dual up- and down-looking longwave IR imaging system that included in-flight calibration capability aboard a Cessna Skymaster shown in Figure 1. The surveys in 2002 and 2003 quantified the horizontal mesoscale variability in the domain around the CBLAST-LOW site near the offshore tower and the horizontal ocean mooring/buoy array throughout the region extending 40-50 km offshore.

Airborne measurements were made of horizontal variability of ocean surface skin temperature using two complimentary infrared (IR) sensors. An AIM model 640Q longwave infrared imager containing a 640 by 512 element QWIP focal-plane detector array sensitive to radiation in the 8-12 µm wavelength range provided high spatial and temporal resolution imagery. High-quality daytime measurements were achieved since the longwave detector minimized solar contamination of the IR imagery. A model KT-15 narrow field-of-view (FOV) radiometer (Heitronics, Wiesbaden, Germany) in the 8-14 µm wavelength range provided calibrated surface temperature at lower resolution. A sky correction was implemented following [*Katsaros*, 1980a] with the corresponding upward-looking AIM imager and KT-15 radiometer. A downward-looking Pulnix model 9701 digital video camera (Pulnix America Inc., Sunnyvale, CA) was used to supplement these measurements. During each flight, the IR imagery was corrected for non-uniformity and calibrated using a model 2004S blackbody (Santa Barbara Infrared Inc., Santa Barbara, CA). The KT-15 radiometers were calibrated pre- and post-experiment in the laboratory, and provided an accurate measurement to compare directly with the calibrated AIM model 640Q imager measurements in-situ during flights.

Figure 1. (Top) Cessna Skymaster flown during CBLAST-LOW 2002/2003 based in Chatham, MA. (Bottom) Close-up of the downward-looking IR imager, collocated video camera, and collocated, narrow FOV IR radiometer.

The IR imager was operated concurrently in two distinct modes identified as Full Frame and Sub-Frame (Averaged) mode. Both modes obtain high spatial resolution and low noise temperature measurements. In the Full Frame mode, complete images were acquired at 1 Hz in order to provide an instantaneous 2-D map of surface temperature with a thermal resolution of roughly 0.02°C. For the nominal altitude of 610 m in 2002 and 875 m in 2003, the spatial resolution was less than 0.3 m and 0.9 m respectively. In the Sub-Frame mode, we sampled the IR imager at a fast frame rate (30 Hz) and then obtained a point measurement by taking the average of a subset of each image. Averaging of a subset of the 327,680 samples in each image reduced the noise and provided a high-resolution spot of the ocean surface. In this Sub-Frame mode, the imager provided a time/spatial series equivalent to a "spot" measurement of temperature with a temperature resolution of less than 0.02°C and a spatial resolution of *O*(1-10m) depending on the altitude and selected image subset matrix.

3. RESULTS

Operating the IR imager in Sub-Frame mode offers a noise level that is significantly below that for an IR radiometer at all spatial resolutions. For example, at the nominal altitude for the 2002 campaign of 610 m, the KT-15 radiometer had a temperature resolution of 0.2°C and a spatial resolution of 80 m compared to 0.03°C and 2.3 m respectively for the longwave IR imager. Our IR system maps the regional SST variability within a 2-hour flight. Maps of sea surface temperature produced using the low-noise, high-resolution data from the longwave IR imager suggest that diurnal warming and tidal advection/mixing force the regional scales of SST. Results from the two weeks of flights in 2002 show that clear skies, strong insolation and moderate wind speeds lead to high SST variability (2.1°C in 10 km). The variability in SST is shown to diminish with the increase in overcast conditions and high wind speed events (1.5°C in 10 km). Measurements from 2003 show similar results with horizontal gradients reaching 4.5°C in 10 km. Repeated flights give us the capability to track the diurnal variability of ocean surface temperature and allow us to determine the extent to which ocean mixing, advection, or heat flux variability is driving this temperature variability.

We estimated the heat flux variability due to ocean skin temperature alone by implementing the TOGA COARE algorithm for the scalar fluxes. The standard expressions for the sensible and latent scalar heat fluxes are

$$Q_s = \rho_a c_p C_h U_{10}(\theta - T_s)$$
$$Q_l = \rho_a L_e C_e U_{10}(q - q_s) \quad (1)$$

where ρ_a is the density of air, c_p is the specific heat of air, U_{10} is the wind speed at 10 m, T_s is the ocean skin temperature, θ is the potential air temperature, L_e is the latent heat of vaporization, q is the water vapor mixing ratio, and q_s is the interfacial value of the water vapor mixing ratio that is computed from the saturation mixing ratio for pure water at T_s. The transfer coefficients for sensible and latent heat, C_h and C_e, are calculated using the TOGA COARE model [*Fairall et al.*, 1996]. Figure 1 shows a map of the sensible and latent fluxes calculated according to (1) using the

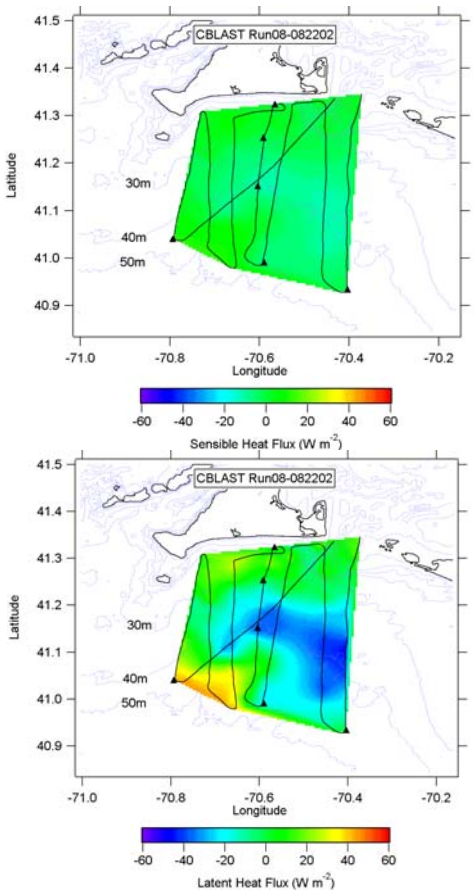

Figure 2. Maps of the sensible (Top) and latent (Bottom) heat flux variability determined using the sea surface temperature measurements produced using the low-noise data from the imager (in Sub-Frame mode). The black trace is the Skymaster flight track and the triangles are the sub-surface moorings deployed during 2002.

map of T_s and the appropriate buoy data. The flight was in the late afternoon on August 22nd 2003 under variably cloudy conditions and a wind speed of 4 m s^{-1}. Figure 2 shows that the variability of the sensible and latent heat fluxes under low wind conditions was ±13.9 and ±52.8 W m^{-2} $10km^{-1}$, respectively. Results from the two weeks of flights during both the summers of 2002 and 2003 demonstrate that the average variability of scalar heat fluxes was ±8.0 W m^{-2} $10km^{-1}$ for the sensible and ±53.6 W m^{-2} $10km^{-1}$ for the latent. The model input parameters (U_{10}, q, θ) were found to be relatively uniform within the CBLAST-LOW study site. Therefore, these results suggest that the heat flux variability is dominated by ocean skin temperature. Heat flux variability of this magnitude is important to the regional estimates of fluxes extrapolated from individual locations since regional flux estimates require an accuracy of better than 10 W m^{-2} [*Fairall et al.*, 1996]. This spatial heat flux variability is also important to the determination of the transfer coefficients since the spatial variability is integrated into the *O*(10km)-footprint of direct covariance flux measurements [*Edson et al.*, 1998].

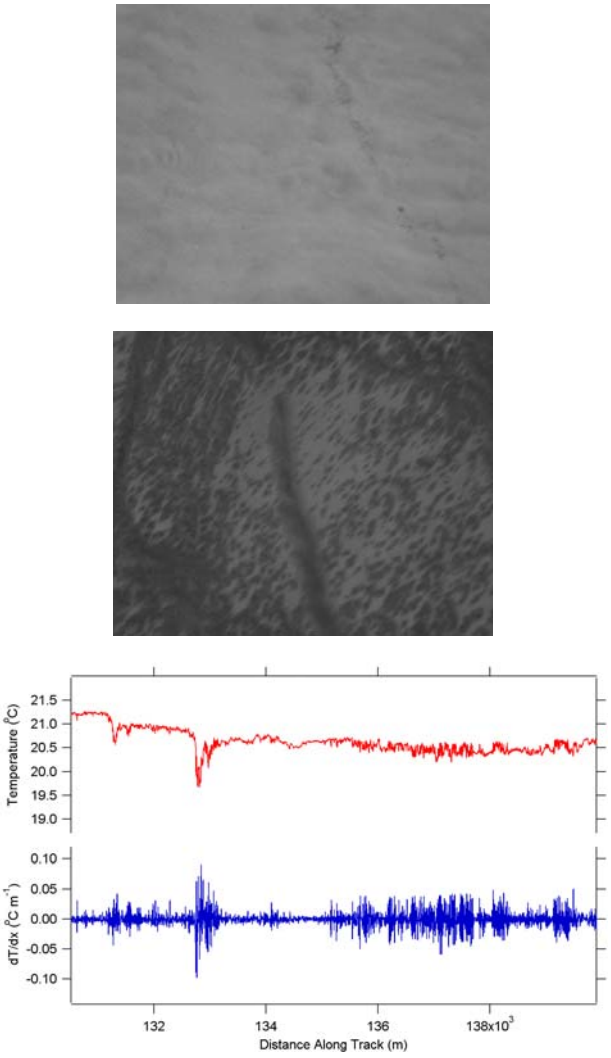

Figure 3. (Top and Middle) Examples of fine-scale IR imagery in Full Frame mode as observed from the aircraft under very low wind speed. Each image is roughly 160 m x 200 m and the top of the images is West. (Bottom) Sub-Frame mode temperature and its derivative measured along the flight track that corresponds to the observations in the Top and Middle images. The Top image is representative of IR imagery data along the flight track between 133.5 – 135 x 10^3 m while the Middle image is of data between 136 – 138 x 10^3 m

Not only do we observe regional variability that is important to air-sea fluxes, but we also observe small-scale structures within the IR imagery (Full Frame mode operation) that suggest mechanisms that drive or enhance exchange under low wind speed conditions. The IR imagery shows high temperature variability on scales of *O*(10m – 1km) under a variety of wind speed conditions.

Figure 3 (Top and Middle) depicts two examples of the infrared signature that are produced during very low wind speeds. These data were taken mid-morning on 8-27-02 with a wind speed less than 1 m s^{-1}. Each image is roughly 160 m x 200 m. The IR image on the Top in Figure 3 shows minimal structure while that in the Middle shows significant spatial variability exhibited by the dark circular blotchy regions. Figure 3 (Bottom) shows the temperature and derivative of the temperature along the track observed during the flight of the observed imagery in Figure 3 (Top and Middle). For the region along the track between 133.5 – 135 x 10^3 m representative of the Top image in Figure 3, the spatial temperature variability is calculated to be 0.004°C m^{-1} and spatial scales of *O*(100m) while for the region between 136 – 138 x 10^3 m representative of the Middle image, the spatial temperature variability is calculated to be 0.013°C m^{-1} and spatial scales less than of *O*(10m). The overall skewness in Figure 3 was observed to be 0.06, suggesting that the temperature variability is Gaussian. This comparison demonstrates the broad range in scales of variability that exist under very low wind speed conditions.

Figure 4 (Top) shows a mosaic of IR images that depicts successive temperature fronts. These data were taken on 8-22-02 in the late afternoon from an altitude of 600 m, which corresponds to a resolution for the imager of roughly 0.3 m. The wind speed was roughly 5 m s^{-1} and the direction was from the SW. An individual IR image is roughly 150 m x 200 m in scale, such that the mosaic is roughly 160 m x 500 m. Lighter shades of gray are warmer temperatures. The variability in temperature across these successive fronts in Figure 4 (Top) is of *O*(0.5 ºC) and the spatial scale between the crests of the fronts are of 77.9 ± 16.6 m. The lack of coherent parallel features in the IR sky imagery suggests that the ocean surface features observed in the downward looking imagery in Figure 4 (Top) are, in fact, real temperature structures. [*Thorpe*, 1988] observed similar coherent structures during stable stratification and suggested the positive skewness was due to "billows" from shear-induced turbulence. Here, the spatial temperature variability is calculated to be 0.009°C m^{-1} and the skewness observed in Figure 4 (Bottom) is 2.8, which is significantly greater than that observed by Thorpe. The crests of these fronts are parallel to ubiquitous visible surface slicks. Comparison to the SCIMS data of N. Frew at WHOI show that the

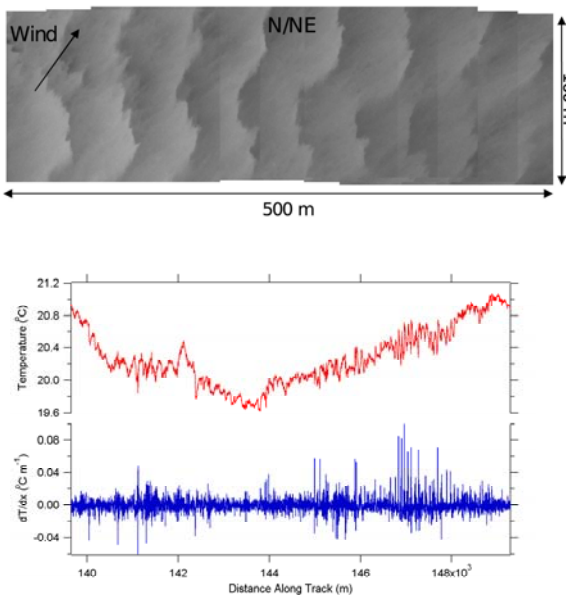

Figure 4. (Top) Mosaic of IR images from Full Frame mode showing the successive fronts of ocean skin temperature in the presence of ubiquitous surface slicks observed on 8-22-02 during a period when the wind was 5 m s^{-1} from the SW. The top of the mosaic is NE. (Bottom) Sub-Frame mode temperature and its derivative measured along the flight track. The coherent ramp structures observed in Top are representative of IR imagery data along the flight track between 146.5 – 148 x 10^3 m.

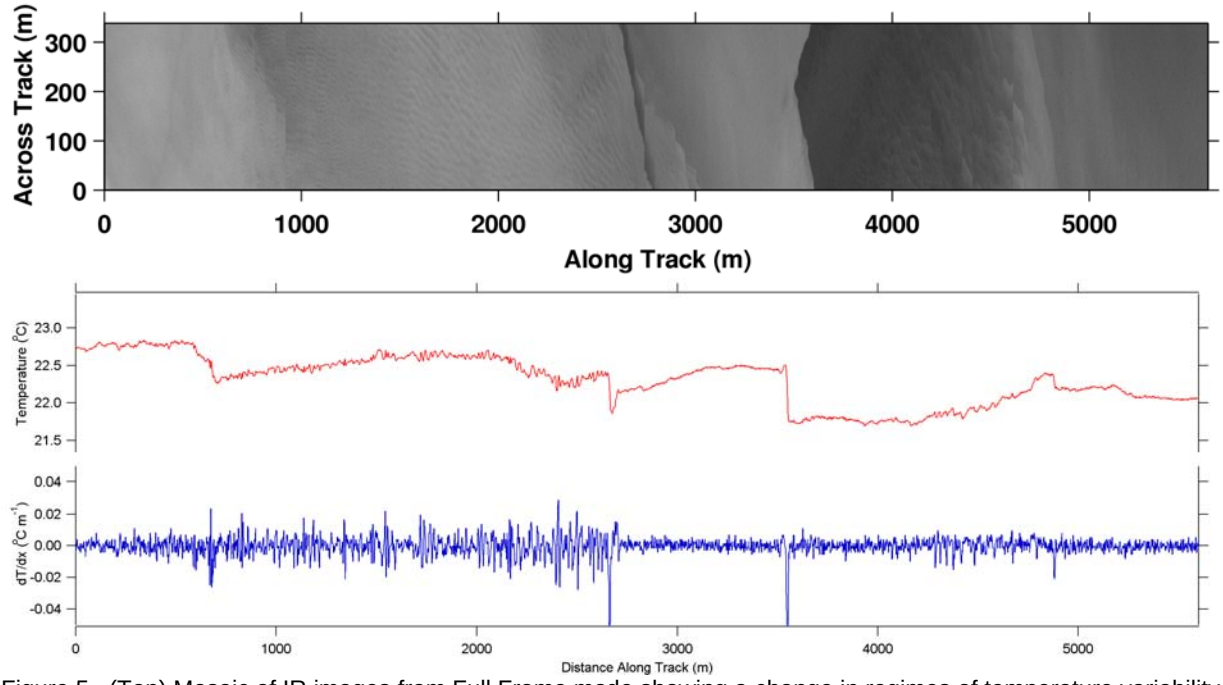

Figure 5. (Top) Mosaic of IR images from Full Frame mode showing a change in regimes of temperature variability across several large-scale temperature fronts observed on 8-14-03 during a period when the wind was 3.4 m s^{-1} from the W. The top of the mosaic is E. (Bottom) Sub-Frame mode temperature and its derivative measured along the flight track.

spatial scales observed in enhancement of ΔCDOM within the microlayer were comparable to those of the coherent ramp temperature structures observed in the airborne IR imagery.

Figure 5 (Top) shows a mosaic of IR images that depicts a change in regimes of temperature variability across several large-scale temperature fronts. These data were taken on 8-14-03 at an altitude of 875 m, which corresponds to a resolution for the imager of roughly 0.9 m. The Skymaster was heading south and the flight track was from left to right in the mosaic. The wind speed was roughly 3.4 m s^{-1} and the direction was from the W. An individual IR image is roughly 350 m x 450 m in scale, such that the mosaic is roughly 350 m x 5600 m. The variability in temperature across these large-scale fronts is observed in Figure 5 (Top) to be of *O*(0.5 ºC) and the spatial scale between the the fronts are of *O*(1 km). Figure 5 (Bottom) shows the temperature and derivative of the temperature along the track

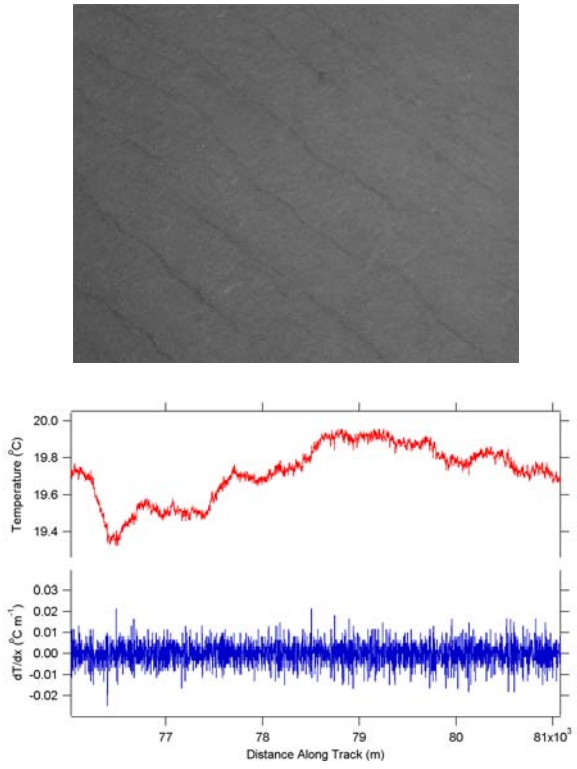

Figure 6. (Top) Example of fine-scale IR imagery as observed from the aircraft under moderate wind speed. Each image is roughly 160 m x 200 m, the top of the images is East, and the wind is from the NE. (Bottom) Temperature and its derivative measured along the flight track that corresponds to the observations in the Top image.

observed during the flight of the observed mosaic in Figure 5 (Top). A field of coherent parallel structures are observed in the IR imagery to the north of the front at 2700 m along the track shows spatial temperature variability to be 0.007°C m^{-1} and spatial scales of 21.7 ± 7.3 m. Between 2700 m and 3500 m along the flight track, little variability exists and is calculated to be 0.002°C m^{-1}. After crossing a sharp temperature front at 3500 m along the flight track, the spatial variability increased to 0.004°C m^{-1}. In this example, distinct regime changes of the spatial variability of SST and their associated coherent structure occur across the passages of fronts.

We also observed the evolution of fine-scale features within the IR imagery during a moderate wind speed period. Figure 6 (Top) shows an IR image (top) taken on 8-28-02 when the wind speed was increasing to 8 m s^{-1} and the direction was from the NE. The image shows an ocean surface that is roughly uniform temperature with very thin bands of cool water that are parallel to the wind and roughly 0.05°C less than the broad regions between the bands. The spacing between these thin cool bands is 28.6 ± 10.2 m. Figure 6 (Bottom) shows the temperature and derivative of the temperature along the track observed during the flight of the observed imagery in Figure 6 (Top). Here, the spatial temperature variability is calculated to be 0.005°C m^{-1} and the overall skewness was observed to be 0.07, suggesting that the temperature variability is Gaussian. These parallel-aligned structures are suggestive of Langmuir circulation. The horizontal spacing of these features increased from 10 m up to 50 m with the increase in fetch offshore and coincided with wind-aligned surface slicks and bubbles visible in the video.

4. SUMMARY

Regional maps of the CBLAST study site using low-noise, high-resolution spatial series of skin temperature show that diurnal warming and tidal advection/mixing control the scales of SST (mean of 2°C $10km^{-1}$) that modulate the heat flux variability (mean of 60 W m^{-2} $10km^{-1}$). Fine-scale imagery of ocean skin temperature elucidated a variety of mechanisms related to atmospheric and sub-surface phenomena that produce horizontal variability over a wide range of scales that decreased with increasing wind speed. Figure 7 summarizes the two years of data taken during CBLAST-Low and shows that the mean fine-scale variability indeed decreases with wind speed.

Under low wind-speed conditions (0 to 2.5 m s^{-1}), the IR imagery shows high temperature variability on scales of *O*(1 m to 100 m) without the distinction of coherent structures. During moderate winds (2.5 to 5 m s^{-1}), we observed extensive regions (*O*(1 km)) of closely-spaced (*O*(10 m)) successive sharp coherent temperature ramps of *O*(1ºC) that coincide with ubiquitous visible surface slicks parallel to the fronts. For wind speeds greater than 5 m s^{-1}, the data show significantly less temperature variability with a high incidence of breaking waves and distinct row/streak structures in the IR imagery that were aligned with the wind and were likely the surface manifestation of Langmuir circulation cells.

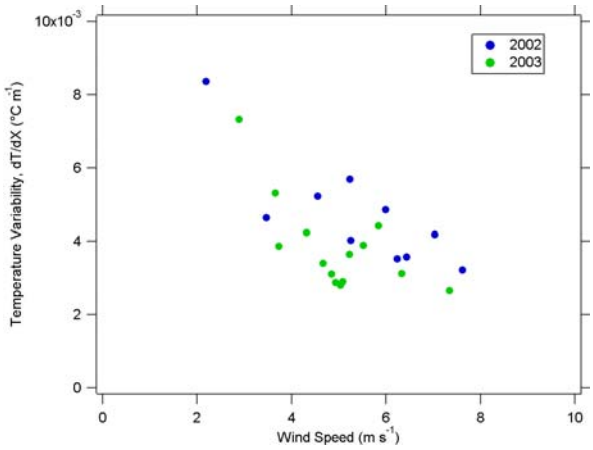

Figure 6. Mean fine-scale variability for each run during the CBLAST-Low experiments of 2002 and 2003.

5. REFERENCES

Edson, J.B., F. Crofoot, W.R. McGillis, and C.J. Zappa, Investigations of flux-profile relationships in the marine atmospheric surface layer during CBLAST, in *16th Symposium on Boundary Layers and Turbulence*, Ref. 8.2, Portland, Maine, USA, 2004.

Edson, J.B., A.A. Hinton, K.E. Prada, J.E. Hare, and C. W. Fairall, Direct covariance flux estimates from mobile platforms at sea, *J. Atmos. Oceanic Tech*, *15*, 1998.

Fairall, C.W., E.F. Bradley, D.P. Rogers, J.B. Edson, and G.S. Young, Bulk parameterization of air-sea fluxes for Tropical Ocean Global Atmosphere Coupled Ocean Atmosphere Response Experiment, *Journal Of Geophysical Research*, *101* (C2), 3747-3764, 1996.

Farrar, J.T., R.A. Weller, C.J. Zappa, and A.T. Jessup, Subsurface expressions of sea surface temperature variability under low winds, in *16th Symposium on Boundary Layers and Turbulence*, Ref. P8.1, Portland, Maine, USA, 2004.

Hagan, D., D. Rogers, C. Friehe, R. Weller, and E. Walsh, Aircraft observations of sea surface temperature variability in the tropical pacific, *Journal of Geophysical Research*, *102* (C7), 15733-15747, 1997.

Jessup, A.T., and V. Hesany, Modulation of ocean skin temperature by swell waves, *Journal of Geophysical Research*, *101* (C3), 6501-6511, 1996.

Jessup, A.T., C.J. Zappa, M.R. Loewen, and V. Hesany, Infrared remote sensing of breaking waves, *Nature*, *385* (6611), 52-55, 1997a.

Jessup, A.T., C.J. Zappa, and H. Yeh, Defining and quantifying microscale wave breaking with infrared imagery, *J. Geophys. Res.*, *102* (C10), 23145-23153, 1997b.

Katsaros, K., Radiative sensing of sea surface temperature, in *Air Sea Interaction: Instruments and Methods*, edited by F. Dobson, L. Hasse, and R. Davis, pp. 293-317, Plenum Press, New York, 1980a.

Katsaros, K.B., The aqueous thermal boundary layer, *Boundary-Layer Meteorology*, *18*, 107-127, 1980b.

McAlister, E.D., and W.L. McLeish, Oceanographic measurements with airborne infrared equipment and their limitations, in *Oceanography From Space*, edited by G.C. Ewing, pp. 189-215, Woods Hole Oceanographic Inst. Rep. No. 65-10, Woods Hole, MA, 1965.

Peltzer, R.D., W.D. Garrett, and P.M. Smith, A remote sensing study of a surface ship wake, *Int. J. Remote Sensing*, *8* (5), 689-704, 1987.

Thorpe, S.A., The dynamics of the boundary layers of the deep ocean, *Science Progress*, *72* (286), 189-206, 1988.

Walsh, E.J., R. Pinkel, D.E. Hagan, R.A. Weller, C.W. Fairall, D.P. Rogers, S.P. Burns, and M. Baumgartner, Coupling of internal waves on the main thermocline to the diurnal surface layer and sea surface temperature during the Tropical Ocean-Global Atmosphere Coupled Ocean-Atmosphere Response Experiment, *Journal of Geophysical Research*, *103* (C6), 12613-12628, 1998.

Zappa, C.J., A.T. Jessup, and H.H. Yeh, Skin-layer recovery of free-surface wakes: Relationship to surface renewal and dependence on heat flux and background turbulence, *Journal of Geophysical Research*, *103* (C10), 21711–21722, 1998.